J Mater Sci (2009) 44:93–101
DOI 10.1007/s10853-008-3109-9

High-damping and high-rigidity composites of Al_2TiO_5–$MgTi_2O_5$ ceramics and acrylic resin

T. Shimazu · H. Maeda · E. H. Ishida · M. Miura · N. Isu · A. Ichikawa · K. Ota

Received: 2 April 2008 / Accepted: 10 November 2008 / Published online: 5 December 2008

Abstract High-damping materials are widely used in engineering fields. In order to increase the precision of vibration control to different levels, high-damping materials with high-rigidity are required. This study attempts to develop a new high-damping high-rigidity material using ductile ceramics based on the Al_2TiO_5–$MgTi_2O_5$ system, which has many continuous microcracks along the grain boundaries. Ductile ceramics have high internal friction ($Q^{-1} = 0.01$–0.037), but very low rigidity (<10 GPa). The rigidity of Al_2TiO_5–$MgTi_2O_5$ ceramics was improved by combining them with a polymer such as acrylic resin. The Young's modulus and internal friction of the composites of Al_2TiO_5–$MgTi_2O_5$ ceramics and acrylic resin are investigated. They show high-damping capacity ($Q^{-1} = 0.03$–0.04) with high rigidity ($E = 50$–60 GPa), and their properties depend on those of the polymer. Thus, the composites fabricated using the above method can serve as high-damping high-rigidity materials.

T. Shimazu · H. Maeda · E. H. Ishida
Graduate School of Environmental Studies, Tohoku University, 6-6-20 Aoba, Aramaki, Aoba, Sendai 980-8579, Japan

T. Shimazu (✉) · M. Miura · N. Isu
General Research Institute of Technology, INAX Corporation, 3-77 Minatomachi, Tokoname, Aichi 479-8588, Japan
e-mail: mazuu@i2.inax.co.jp

A. Ichikawa
Sanwa Yuka Kogyo Co., Ltd, Ichiriyamacho, Kariya, Aichi 448-0002, Japan

K. Ota
Q INVERSE Incorporated, Mino, Osaka 562-0001, Japan

Introduction

Vibration control technology has been widely used in various engineering fields, such as manufacturing of machines and cars and in construction. Damping technology is one of the most common techniques for vibration control, for example, conventional mechanical dampers (air damper and oil damper) and high-damping materials have been widely used in many systems. Recent technological advancements in the field of engineering require the processing and measurement of extremely minute areas as well as miniaturization and weight reduction of equipment [1, 2]. Hence, from this viewpoint, vibration control technologies require not only usual methods, but also a new high precision vibration control system [3, 4]. In order to fulfill this requirement, a high-damping material with high rigidity has been developed as a structural material for machines. This material is expected to increase the damping property of the system and leads to a reduction in the weight of the equipment, while simplifying the design of the machine, reducing costs, and the number of parts [3, 4].

Polymers such as rubbers and elastomers have been widely used as damping materials; however, their rigidity is not sufficient for mechanical use. Structural materials must have high rigidity; however, the damping capacity of high-rigidity materials is generally quite low. Thus, it can be noted that there is a trade-off between rigidity and damping. Nevertheless, several studies have attempted to increase the damping property of high-rigidity materials, particularly metallic materials [5–8]. High-damping steel is composed of a metallic plate and a polymer and is well known as a high-damping and high-rigidity material that can be used for multiple purposes such as in the construction of the bodies of cars, trains, and ships. However, the high-damping steel has some disadvantages such as the

limitation of possible shapes and forms. Other high-damping metallic materials such as a high-damping Mn–Cu alloy and a shape memory alloy have also been developed and used [5–8]. The production of high-damping alloys requires highly accurate process control. In addition, these alloys have limited usage in environments with a magnetic or electric field. Thus, from the point of view of the industry and manufacturing, it is important to develop a high-damping material that has high heat resistance, chemical stability, isolation, and non-magnetism, such as ceramic, by a simple method.

In general, ceramics have high rigidity; their inner structure hardly changes at room temperature. The damping property (internal friction) of ceramics is lower than that of polymers and metals [9]. Most studies that have been published have described the internal friction of ceramics as a parameter for the evaluation of the change in the inner structure at high temperature [10–16], whereas only a few studies have reported that ceramic damping materials can be used at room temperature [17–20].

Previous studies [21–23] have attempted to increase the ductility of ceramics in order to improve their brittleness, which is one of their major defects. Although there is a trade-off between rigidity and flexibility in the case of ceramics, the authors have been able to develop ductile ceramics based on the Al_2TiO_5–$MgTi_2O_5$ system by controlling the microstructure [23]. The microstructure of Al_2TiO_5–$MgTi_2O_5$ ceramics (porosity: approximately 10%) is shown in Fig. 1. Many elongated columnar grains and interconnected microcracks were formed. The ductile Al_2TiO_5–$MgTi_2O_5$ ceramics show large plastic deformation (Fig. 2) due to flexural force caused by the integration

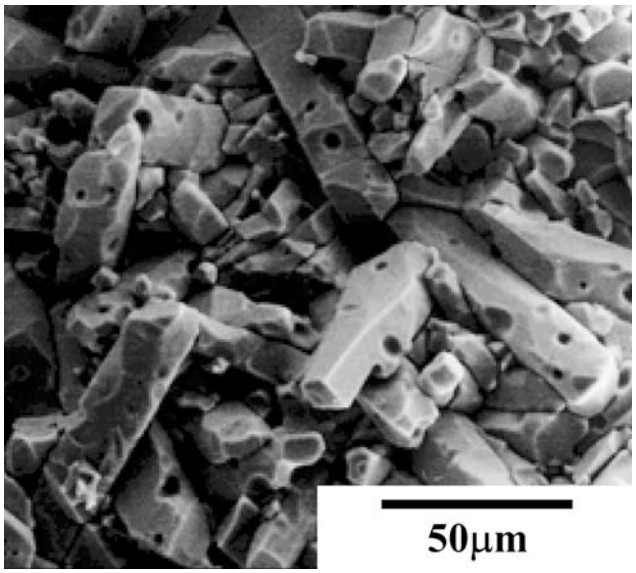

Fig. 1 Cross-sectional view of the fractured surface of the solid solution $Mg_{0.25}Al_{1.5}Ti_{1.25}O_5$

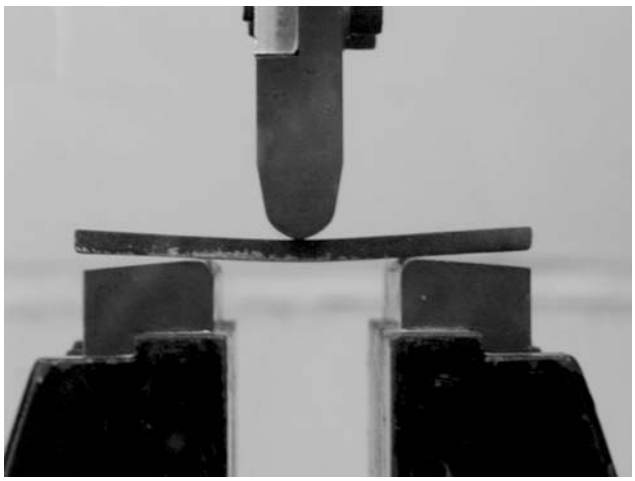

Fig. 2 Large distortion displayed during flexural strength measurement

of small displacements at the grain boundaries due to the pull-out mechanism of the grains for reduction in strain [23]. These movements cause mechanical friction at the surface of the grains, which results in high internal friction [23]. The internal friction in ceramics is equivalent to that in polymers and is much higher than that in other common oxide ceramics such as alumina (porosity of 30%, internal friction of 2.0×10^{-4}) and mullite (porosity of 25%, internal friction of 1.5×10^{-3}) [23]. It is expected that ductile ceramics will be used as damping materials due to their high internal friction. However, in practice, Al_2TiO_5–$MgTi_2O_5$ ceramics have some disadvantages such as low rigidity; detachment of the grains from the ceramic body, which is based on its ductility; and many microcracks between the grains. In particular, the very low rigidity of these ceramics needs to be significantly improved. Therefore, in general, there is a trade-off between rigidity and damping properties [5, 24]. Hence, it is difficult to increase the rigidity without decreasing the internal friction.

In this study, the low rigidity of ductile Al_2TiO_5–$MgTi_2O_5$ ceramics was tried to improve by a simple method, e.g., combination with other materials. The material for impregnating the ceramic should have a relatively low rigidity compared with the ceramic and must be introduced into the microcracks of the matrix. It is important to ensure that the grains of the composite are not bound very tightly by the impregnated material after the combination process. A polymer was selected as the combining material based on its low rigidity and easy handling ability. In this study, general-purpose low-viscosity thermosetting acrylic resins were used and the method of impregnation after vacuum and heat curing was selected to produce the composites. Impregnation is a preferable way to introduce the polymer into pores with dimensions of the order of submicrons. The change in the

Young's modulus and the internal friction of the Al_2TiO_5–$MgTi_2O_5$ ceramics after combining them with acrylic resin were investigated. The effect of the properties of the polymer on those of the composites was also studied.

Experimental

Fabrication of composites of Al_2TiO_5–$MgTi_2O_5$ ceramics and acrylic resin

In the Al_2O_3–TiO_2–MgO system, aluminum titanate oxide (Al_2TiO_5) forms a solid solution [25–27] with magnesium titanate oxide ($MgTi_2O_5$), which has the same crystal structure [28, 29]. In this study, seven different solid solution compositions were prepared (Fig. 3). The compositions are labeled a–g in Table 1. Raw powders of Al_2O_3 (AL-160SG-4: Showa Denko K·K.), TiO_2 (KA-10C: Titan Kogyo Co., Ltd.), and MgO (#500: Tateho Chemical Industries Co., Ltd.) were mixed with ethanol in appropriate amounts in a plastic ball mill for 20 h. After drying the slurry, the resulting powders were pressed in a die at 50 MPa such that their dimensions were 80 × 12 × 5 mm^3. They were subsequently fired at 1500 °C for 2 h.

The composites of the Al_2TiO_5–$MgTi_2O_5$ ceramics and acrylic resin were prepared as follows. Acrylic resin was introduced into the ceramic pores by a vacuum impregnation

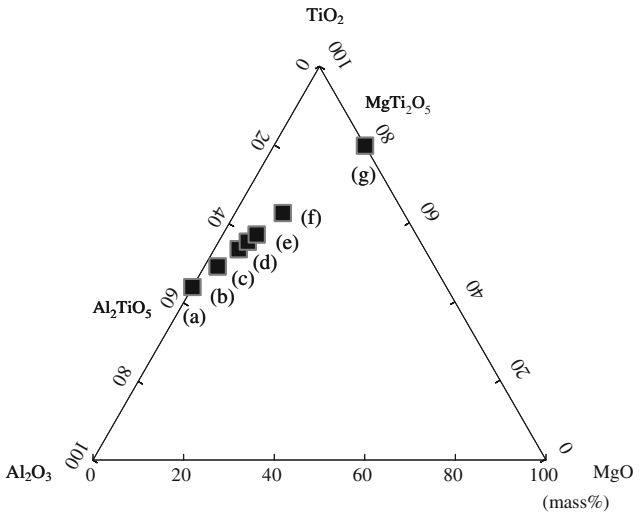

Fig. 3 Composition of the specimen used in the Al_2TiO_5–$MgTi_2O_5$ system

Table 1 Compositions of Al_2TiO_5–$MgTi_2O_5$ in the specimens

Sample	a	b	c	d	e	f	g
Al_2TiO_5 (mol%)	100	87	75	70	65	50	0
$MgTi_2O_5$ (mol%)	0	13	25	30	35	50	100

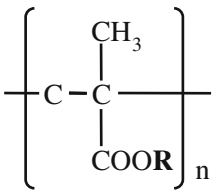

Fig. 4 Molecular structure of the acrylic resin

method. Since the pore size of the ceramics varied from 0.1 to 1 μm [23], it was ensured that the viscosity of the acrylic resin was sufficiently low to impregnate the pores. In this study, low-viscosity acrylic resin liquids ($\eta = 0.07$ Pa s at room temperature) were selected, which were easy to handle and could be cured by heating. Figure 4 shows the molecular structure of the resins. Two types of acrylic resins with different degrees of hardness and internal friction (A: hard acrylic resin, storage modulus $E' = 0.17$ GPa, $\tan\delta = 0.11$; B: soft acrylic resin, storage modulus $E' = 0.01$ GPa, $\tan\delta$=0.65) depending on the side chain (A: short side chain, $R = CH_3$, B: long side chain, $R = C_nH_{2n+1}$ ($n = 12$, 13)) were used. After the acrylic resin liquid was saturated into the pores, it was cured with the ceramics at 80 °C for 2 h.

Evaluation

The Young's modulus and internal friction of the composites were measured by the free resonance method (Nippon Techno-plus Co., Ltd.: JE-RT). Figure 5 shows a schematic diagram of the free resonance method. The specimen was placed on stainless steel wires (ϕ = 50 μm) at the node of vibration. The noncontact electrostatic transmitter produced a vibration in the specimen, and the resonance frequency was determined by detecting the vibration amplitude by the sonic sensor while shifting the oscillation frequency. Since the ceramic specimen did not have electrical conductivity, its surface was coated with thin carbon paint that provided electrical conductivity. The internal friction (Q^{-1}) was calculated as shown in Fig. 6 by

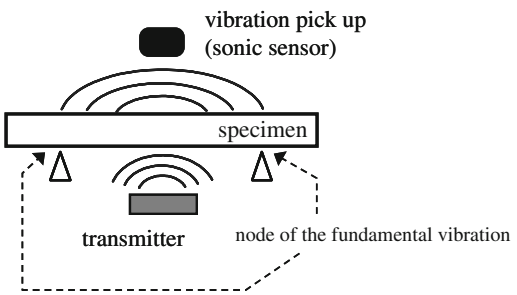

Fig. 5 Free resonance method for the measurement of the Young's modulus and internal friction

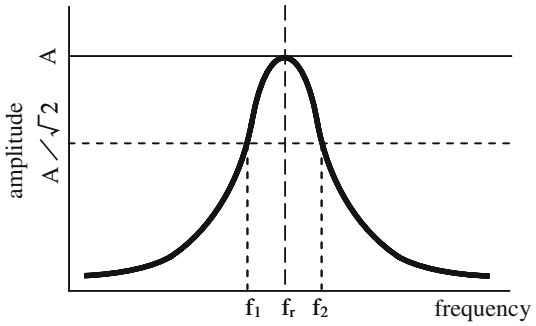

Fig. 6 Diagram of measurement for half-power bandwidth method

the half-power bandwidth method using Eq. 1 [9, 30, 31] (f_r, resonance frequency (Hz), f_1 and f_2, frequencies where the amplitude is $1/\sqrt{2}$ of the maximum vibration amplitude (Hz)).

$$Q^{-1} = \frac{f_2 - f_1}{f_r}. \quad (1)$$

The Young's modulus was calculated by the following equation [10] (f_r, resonance frequency (Hz); l, length (mm); t, thickness (mm); W, width (mm); m, weight (g)):

$$E = 0.9468 \times 10^{-9} \times \frac{l^3 m}{t^3 W} \times f_r^2. \quad (2)$$

The flexural strain σ (%) was calculated using the following equation with the three-point bending test data (D, deflection deformation (mm); S, span (mm); t, thickness (mm)).

$$\sigma = \frac{6Dt}{S^2} \times 100. \quad (3)$$

The porosity was calculated from the bulk density and the absolute specific gravity. The pore size distribution was measured by mercury intrusion porosimetry. The microstructure of the fractured cross section was observed by a standard electron microscope (scanning electron microscope).

Results and discussion

Impregnation state of the composites

In this section, the phase where the acrylic resin impregnated the pores of the ceramics was discussed. A secondary electron image of the solid solution (*e*) is shown in Fig. 7a and the backscattered electron images of the ceramic are shown in Fig. 7b. In Fig. 7b, there are several areas that are approximately 5–10 μm in size with a dark color indicating the existence of light elements. Using electron probe microanalysis, it is observed that this dark area, which contains a large amount of elemental carbon, indicates the presence of acrylic resin, as shown in Fig. 8. The porosity and distribution of the pore size of the solid solution (c) and its composites with acrylic resins A and B are shown in Fig. 9 and Table 2, respectively. Both acrylic resins A and B caused a large decrease in the porosity; the main pores, including finer pores with a diameter of less than 1 μm, also showed a decrease in size. These results indicate that the acrylic resin impregnated almost all the finer pores.

Young's modulus and internal friction of the composites

The change in the Young's modulus of the Al_2TiO_5–$MgTi_2O_5$ ceramics due to the combination with acrylic resin is shown in Fig. 10. After the combination, the Young's modulus of the composites increased to more than 50 GPa, which is about 5–50 times higher than that of the base ceramics. The increase in the Young's modulus of the composites obtained with the hard acrylic A was greater than that observed after using the soft acrylic resin B.

Before the combination, the Al_2TiO_5–$MgTi_2O_5$ ceramics had a very low value of Young's modulus that was <10 GPa; the Young's modulus was low presumably because of the unique microstructure, which was heavily microcracked. Figure 11 shows the stress–strain curve of the solid solution (d) measured with the three-point bending test. Although the stress increased, the slope

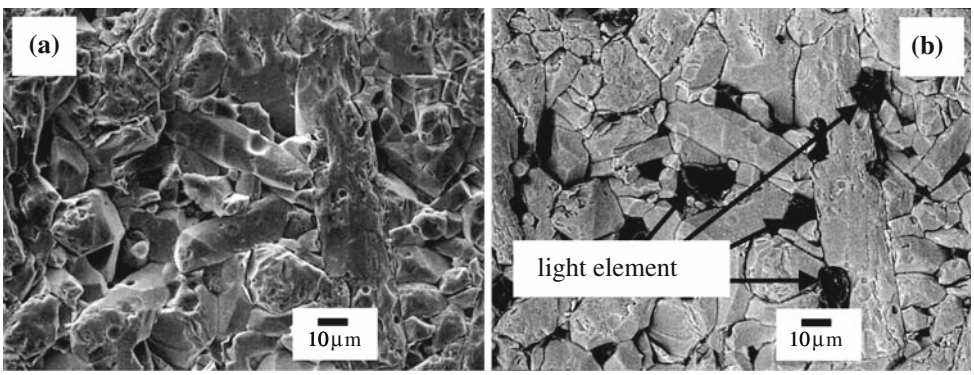

Fig. 7 Scanning electron image (SEI) of the cross section of the composite of the solid solution. $Mg_{0.35}Al_{1.3}Ti_{1.35}O_5$ and polymer A. Figure 6a and b shows the SEI and the backscattered electron image, respectively

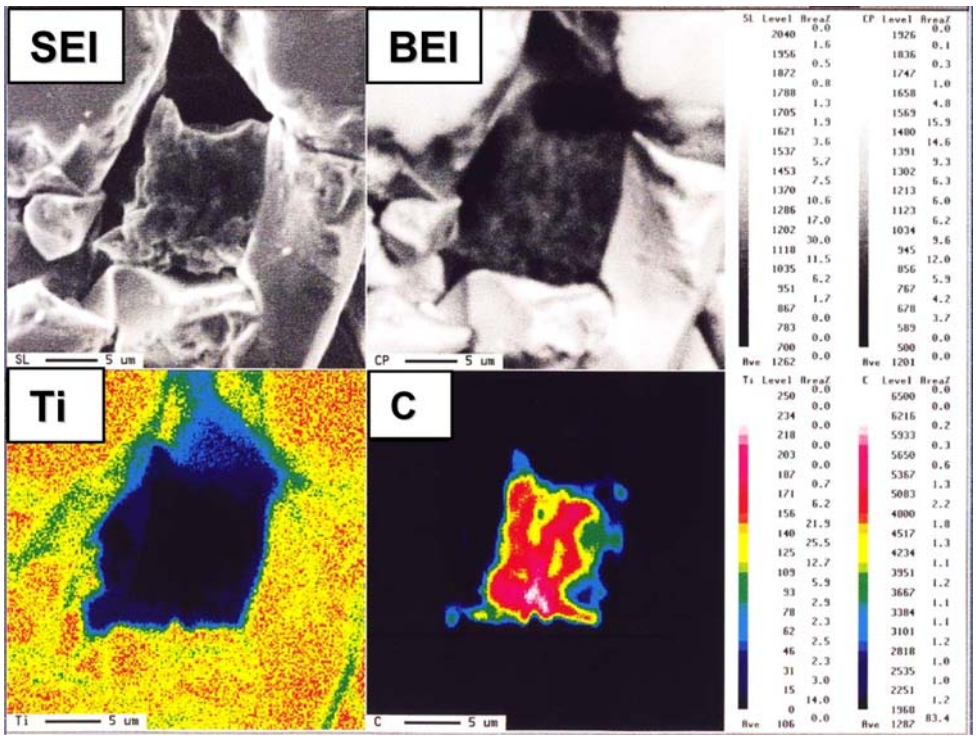

Fig. 8 Electron probe microscope image of the cross section of the composite of $Mg_{0.35}Al_{1.3}Ti_{1.35}O_5$ and polymer A. The SEI, backscattered electron image (BEI), image of the titanium element (Ti), and the image of the carbon element (C) are shown in the figure

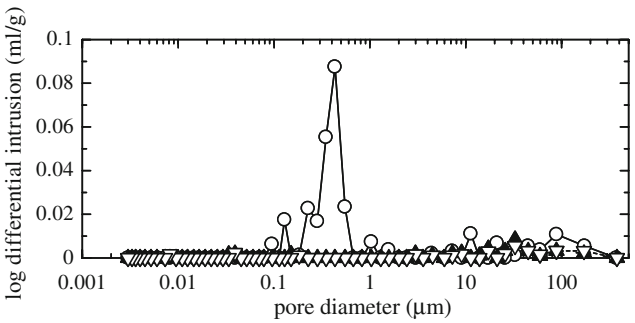

Fig. 9 Pore size distribution of the composites of Al_2TiO_5–$MgTi_2O_5$ and the polymers. The symbols (◯), (▽), and, (▲) indicate $Mg_{0.35}Al_{1.3}Ti_{1.35}O_5$, and its composites with polymers A and B, respectively

Table 2 Porosity of Al_2TiO_5–$MgTi_2O_5$—polymer composites

Sample	Porosity (%)
$Mg_{0.35}Al_{1.3}Ti_{1.35}O_5$	10.5
$Mg_{0.35}Al_{1.3}Ti_{1.35}O_5$—polymer A composite	1.8
$Mg_{0.35}Al_{1.3}Ti_{1.35}O_5$—polymer B composite	1.8

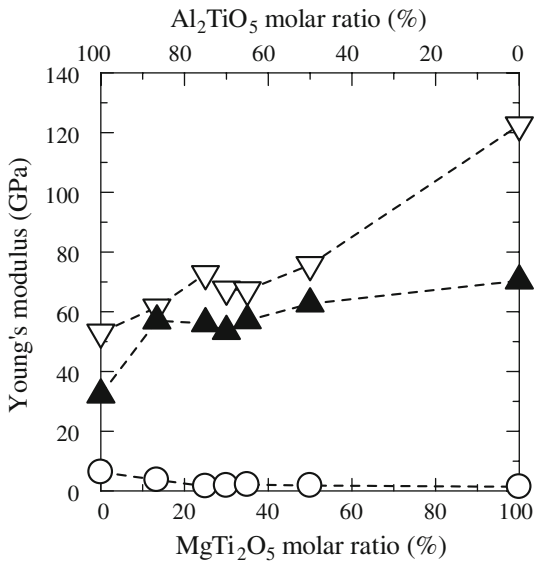

Fig. 10 Influence of the combination of the polymer and Al_2TiO_5–$MgTi_2O_5$ ceramics on Young's modulus. The symbols (◯), (▽), and, (▲) indicate the base ceramics and their composites with polymers A and B, respectively

decreased with the strain; a nonlinear relation between the stress and the strain was observed. The Al_2TiO_5–$MgTi_2O_5$ ceramics had many microcracks along the grain boundaries, which were formed due to a reduction in the thermal stress related to the thermal expansion anisotropy of the elongated grains during the cooling process [32]. In this material, the bonding strength of most of the grain boundaries was very weak; the ceramics can be regarded as composites with the cavities at the grain boundary as a constituent phase with zero stiffness. As in our previous study [23], the ductility of the ceramics under flexural stress was ascribed to the pull-out mechanism of the columnar grains. Thus, in this study, the measured value of the Young's modulus of the Al_2TiO_5–$MgTi_2O_5$ ceramics was the apparent value. Young's modulus

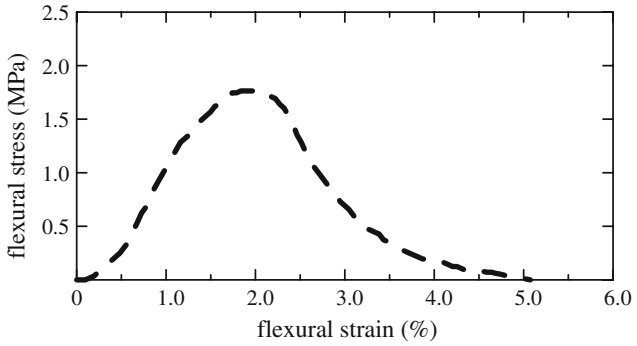

Fig. 11 Stress–strain curve of the solid solution $Mg_{0.3}Al_{1.4}Ti_{1.3}O_5$ in three-point bending test

is an elastic parameter used to measure elastic strain, but in this material, the measured value is not reflecting the correct elastic properties because the strain with external force included the strain induced by the slippage of the grains due to the microcracks along the grain boundaries.

A significant improvement in the Young's modulus was obtained when the acrylic resin impregnated the cavities along the grain boundaries. The influence of the combination of the ceramics and acrylic resin on the stress–strain curves of the Al_2TiO_5–$MgTi_2O_5$ ceramics are shown in Fig. 12. The stress on the composites increased more rapidly than that on the base ceramics; the stiffness was improved by the combination. Figure 13 shows the variation in the maximum flexural strain at maximum flexure stress of the Al_2TiO_5–$MgTi_2O_5$ ceramics after combination with the acrylic resin. The base ceramics (b–f) showed a very large strain because of a weak bond between the grains due to the formation of many microcracks along the grain boundaries. After the combination, both types of resins caused a significant decrease in the bending strain. The increase in the resistance to deformation indicates that the movable grains in the ceramics were firmly fixed by the resin that impregnated the cavities along the grain boundaries. In Fig. 13, it can be observed that the bending strains of the composites

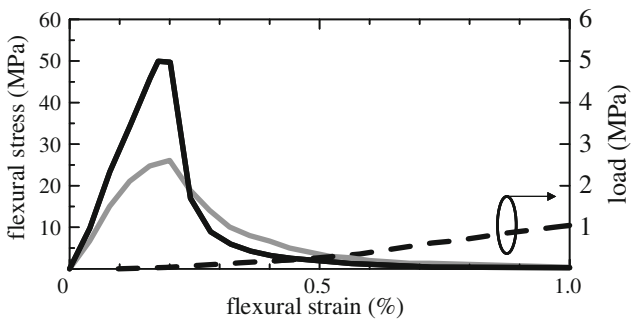

Fig. 12 Influence of the combination of the polymer and the solid solution $Mg_{0.3}Al_{1.4}Ti_{1.3}O_5$ (– – –) on the stress–strain curve. The symbols (▬) and (▬) indicate the composites of $Mg_{0.3}Al_{1.4}Ti_{1.3}O_5$ with polymers A and B

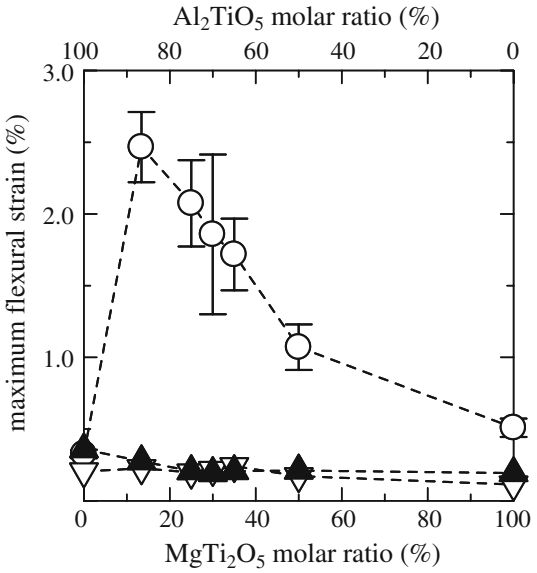

Fig. 13 Influence of the combination of the polymers and Al_2TiO_5–$MgTi_2O_5$ ceramics on the maximum flexural strain. The symbols (◯), (▽), and, (▲) indicate the base ceramics and their composites with polymers A and B, respectively

produced with acrylic resins A and B were almost comparable; however, a difference was observed in the behavior of the stress–strain curves in Fig. 12. For the composite with the acrylic resin A, the stress increased almost proportionally with the strain and the slope of the curve was larger than that of the curve of acrylic resin B. The function of the acrylic resin was to prevent the displacement of the grains with external force and to increase the elastic limit between the disconnected ceramic grain boundaries. The higher storage modulus of the impregnated acrylic resin increased the elasticity of the cavities at the grain boundaries; the bulk property of the composites was strongly affected by the properties of the acrylic resin.

Figure 12 shows the nonlinear behavior of the stress and the strain for acrylic resin B; the slope of the curve decreased while the stress increased with strain, and then the stress decreased gradually. It can be inferred that the decrease in the stress was caused by the deformation of the impregnated resin or plastic deformation caused by the sliding displacement of the ceramic grains along the grain boundaries. Figure 12 shows that both the composites did not display fractures due to brittleness and the stress was slowly decreased particularly in the composite with acrylic resin B. The plastic deformation might have occurred after reaching the maximum stress, and the relaxation behavior in the previous stage could have been caused by the decrease in the deformation of the acrylic resin. However, to verify this inference, further studies are required.

During the measurement of the Young's modulus, the measured value of the Al_2TiO_5–$MgTi_2O_5$ ceramics was the

apparent value because of the existence of weak and partial bonds at the grain boundaries due to many microcracks formed in the matrix. For the same reason, previous studies also could not obtain an accurate value of the Young's modulus for Al_2TiO_5–$MgTi_2O_5$ ceramics. The authors attempted to estimate the Young's modulus of the Al_2TiO_5–$MgTi_2O_5$ ceramics from the composite based on the rule of mixtures. The composites of the Al_2TiO_5–$MgTi_2O_5$ ceramics and acrylic resin were prepared by the impregnation of the resin into the porous ceramics. In the base ceramics, which was different from common brittle ceramics, the ceramic grains were not bound tightly at the boundaries of the grains. Thus, the composites can be recognized as a fiber-reinforced material which is the large elongated ceramic grain fillers were dispersed and densely packed (about 90 vol.%) into the small amount of acrylic resin matrix (about 10 vol.%), rather than the usual porous ceramic–polymer composites.

In general, the Young's modulus of a fiber-reinforced composite is frequently discussed based on the rule of mixtures. Although the approximation formula should be experimentally determined, in this study, the most elementary equation 4 was used for estimation. (E_c, Young's modulus of the composite (GPa); V_f, volume fraction of fiber (vol.%); E_f, Young's modulus of fiber (GPa); V_m, volume fraction of matrix (vol.%); E_m, Young's modulus of matrix (GPa)).

$$E_c = V_f E_f + V_m E_m. \quad (4)$$

The Young's moduli of the Al_2TiO_5–$MgTi_2O_5$ ceramic grains were estimated to be at least more than 65–135 or 60–80 GPa when acrylic resins A and B are used, respectively. The Al_2TiO_5–$MgTi_2O_5$ ceramic grains initially have high rigidity, thus the high rigidity of the composites was provided by the stiffness of ceramic grains mostly and the impregnating resin increased the elasticity limit between the grains.

Next, the internal friction of the composites was discussed. The change in the internal friction of the Al_2TiO_5–$MgTi_2O_5$ ceramics after combining them with the acrylic resin is shown in Fig. 14. The effects of the combination were different depending on the properties of the resin. When acrylic resin A was used, the internal friction for every composition decreased to a common value of around 0.016, which was approximately equivalent to the value for common damping materials such as lead and cast iron [30, 33]. This behavior was assumed to be caused by a decrease in the strain due to the displacement of the grains caused by the impregnated resin. Less displacement decreased the mechanical friction at the grain boundaries and grain-resin boundaries. On the other hand, when acrylic resin B was used, it increased the internal friction, although the composites showed less strain by external forces, and the variations in the behavior of the internal friction of the composites were similar to those of the base ceramics. Figure 12 shows the result of the nonlinear correlation between the stress and the strain when resins with a low-storage modulus were used. From this result, the increase in the internal friction was attributed to the decrease in the external force caused by the deformation of the resin.

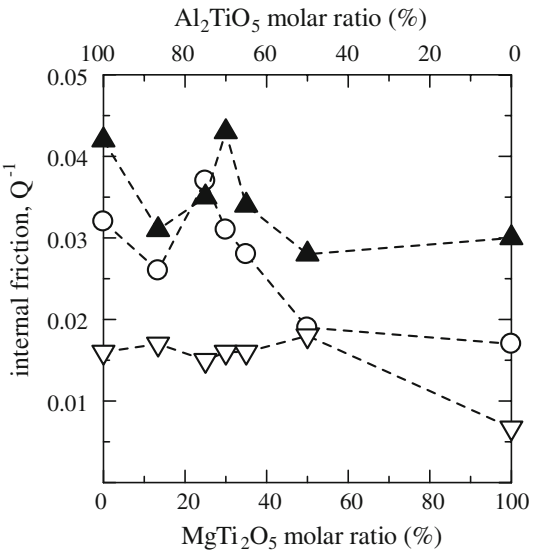

Fig. 14 Influence of the combination of the polymers and Al_2TiO_5–$MgTi_2O_5$ ceramics on internal friction. The symbols (◯), (▽), and, (▲) indicate the base ceramics and their composites with polymers A and B, respectively

Influence of the properties of acrylic resin

The influence of the properties of the acrylic resin on the Young's modulus and internal friction of the composites was investigated. Five types of acrylic resins A–E with different values of the storage modulus (E') and tan δ due to differences in their side chains are listed in Table 3.

Table 3 Storage modulus and internal friction of the impregnated polymer

	A	B	C	D	E
Side chain	$-CH_3$	$-C_nH_{2n+1}$ $(n=12,13)$	$-CH_2(C_4H_7O)$	$-(C_2H_4O)_2H$	$-(C_2H_4O)_8H$
Storage modulus (E', GPa)	0.17	0.012	0.21	0.072	0.0049
Internal friction (tan δ)	0.11	0.65	0.47	0.48	0.19

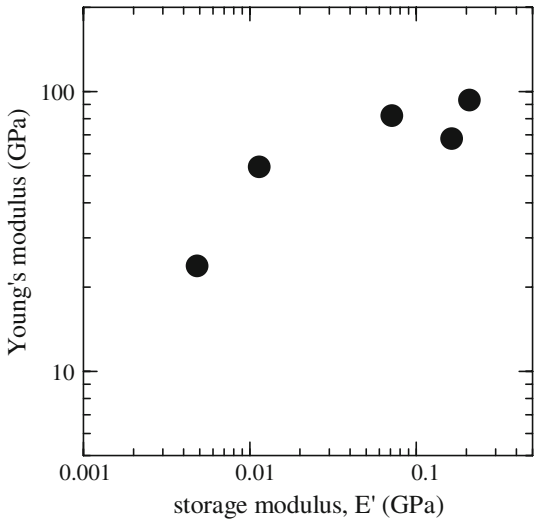

Fig. 15 Influence of the storage modulus of the polymer on the Young's modulus of the composites of $Mg_{0.3}Al_{1.4}Ti_{1.3}O_5$ and the polymers

These resins were combined with the solid solution $Mg_{0.3}Al_{1.4}Ti_{1.3}O_5$. The Young's modulus of the composites increased with E' of the impregnated acrylic resin, as shown in Fig. 15. On the other hand, the internal friction decreased with E', as shown in Fig. 16. The storage modulus was verified as the most important principal factor which affects the composites properties (Young's modulus, internal friction). In contrast, the correlation between the tan δ of acrylic resin and the composites properties was not observed.

These results indicate that the properties of the composites, such as the Young's modulus and internal friction, can be controlled by the storage modulus of the

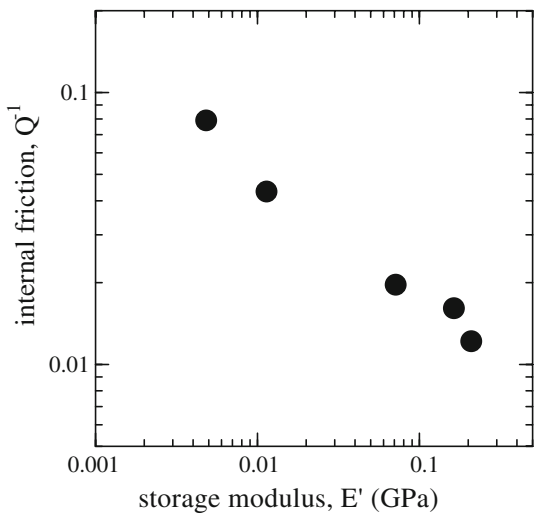

Fig. 16 Influence of the storage modulus of the polymers on the internal friction of the composites of the $Mg_{0.3}Al_{1.4}Ti_{1.3}O_5$ and the polymers

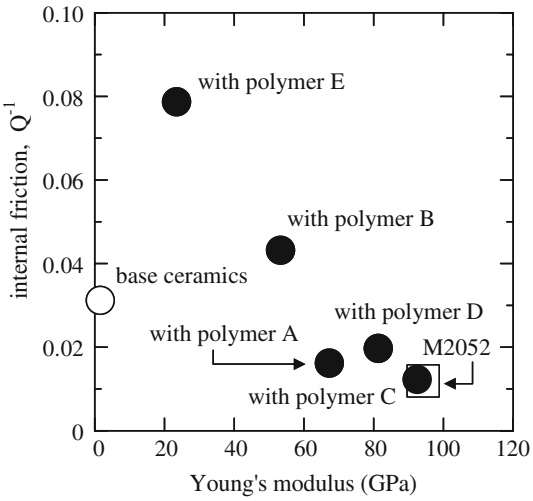

Fig. 17 Variation in the Young's modulus and internal friction due to the combination of diverse acrylic resins with $Mg_{0.3}Al_{1.4}Ti_{1.3}O_5$. The rigidity and damping of the composite with polymer C were approximately equal to those of M2052, which is a typical high-damping alloy (marketed production)

impregnated resin. The variation in the Young's modulus and internal friction due to the combination of the acrylic resins A–E with $Mg_{0.3}Al_{1.4}Ti_{1.3}O_5$ is shown in Fig. 17. There is a trade-off between the Young's modulus and the internal friction. The values of these parameters vary in accordance with the resins. Appropriate selection of the impregnating material will enable to control the properties of the composite. In the case of acrylic resin C, the Young's modulus and the internal friction of the composites were almost equal to those of M2052, which is a typical high-damping alloy (T. Shimazu, unpublished data, 2007). Thus, the combination of the Al_2TiO_5–$MgTi_2O_5$ ceramics and acrylic resin can be effectively used for the fabrication of a high-damping high-rigidity material.

The properties of the composites would be affected not only by the storage modulus of the impregnated resin, but also by other factors such as the wettability and boundary adhesion between the ceramics and the acrylic resins. Further studies will be required to clarify the effect of the combination of Al_2TiO_5–$MgTi_2O_5$ ceramics and acrylic resin on the Young's modulus and internal friction.

Conclusions

The Young's modulus of the high-damping ductile Al_2TiO_5–$MgTi_2O_5$ ceramics was improved by combining them with acrylic resin. The Young's modulus and internal friction were changed depending on the storage modulus of the acrylic resin; the storage modulus was determined on the basis of the increase in the elastic limit between the disconnected ceramic grain boundaries due to the

impregnation of acrylic resin. The higher the storage modulus of the acrylic resin, the larger was the increase in the Young's modulus of the composite. The acrylic resin with a low-storage modulus caused an increase in both the Young's modulus and internal friction. The acrylic resin was appropriately selected so that the Young's modulus and the internal friction of the composites were approximately equal to those of M2052, which is a typical high-damping alloy. Thus, the combination of the Al_2TiO_5–$MgTi_2O_5$ ceramics and the polymer was shown to be effective in the fabrication of a material having high-damping and high-rigidity.

Acknowledgement This study was supported by the Ministry of Economy, Trade and Industry for Regional Consortium Research Development Work 2003–2005, and by a Grant-in-Aid for Scientific Research from the Japan Society for the Promotion of Science (No. 18201014).

References

1. Igata N (2004) Kinzoku 74:237
2. Kawahara K, Yin F (2003) Seishin Corp Technical Report
3. Kawahara K (2006) Key Eng Mat 319:217
4. Igata N, Nishiyama K, Ota K, Yin Y, Wuttig W, Golovin IS, Humbeeck JV, San Juan J (2003) J Alloys Compd 355:230
5. Sugimoto K (1974) Trans Iron Steel Inst Jpn 60:2203
6. Hedley JA (1968) Metall Sci J 2:129
7. Yin F, Ohsawa Y, Satoh A, Kawahara K (1998) Z Metallkd 89:481
8. Fukuhara M, Yin F, Ohsawa Y, Takamori S (2006) Mater Sci Eng A 442:439
9. Fantozzi G (2001) In: Schaller R, Fantozzi G, Gremaud G (eds) Mechanical spectroscopy of Q^{-1} 2001: with applications to materials science. Mater science forum. Trans Tech Pub. Ltd., Zürich, p 3
10. Matsushita K, Kuratani S, Okamoto T, Shimada M (1984) J Mater Sci Lett 3:345
11. Pezzotti G, Ota K (1997) J Ceram Soc Jpn 105:1
12. Basu B, Donzel L, Van Humbeeck J, Vleugets J, Schaller R, Van Der Biest O (1999) Scr Mater 40:759
13. Pezzotti G, Ota K (1998) Phys Rev B 58:11880
14. Takata S, Ueno S, Kawakami Y, Akatsu T, Tanabe Y, Yasuda E, Waku Y (2001) J Ceram Soc Jpn 109:561
15. Nishimura H, Ikuhara Y, Ota K, Pezzotti K (2002) Mater Trans 43:1552
16. Sato S, Serizawa H, Araki H, Noda T, Kohyama A (2003) J Alloys Compd 355:142
17. Matsushita K, Okamoto T, Shimada M (1985) J Phys 46:549
18. Fang QF, Liu T, Li C, Wang XP, Zhang GG (2006) Key Eng Mater 319:167
19. Fantozzi G, Bourim EM, Kazemi S (2006) Key Eng Mater 319: 157
20. Lambrinou K, Van der Biest O, Lube T, Tassini N, Patsias S, Chalvet F, Portu G (2007) J Eur Ceram 27:1307
21. Shimazu T, Miura M, Isu N, Ogawa T, Ichikawa A, Ishida EH (2006) Proceedings of 3rd water dynamics, Sendai, Japan, p 69
22. Shimazu T, Miura M, Kuno H, Isu N, Ota K, Ishida EH (2006) Key Eng Mater 319:173
23. Shimazu T, Miura M, Isu N, Ogawa T, Ota K, Maeda H, Ishida EH (2008) Mater Sci Eng A 487:340
24. Ashby MF (1992) Materials selection in mechanical design. Pergamon Press Ltd, Oxford, p 109
25. Berezhnoi AS, Gul'ko NV (1955) Ukrain Khim Zhur 21(2):158
26. Cleveland JJ, Bradt RC (1978) J Am Ceram Soc 61:478
27. Boden P, Glasser FP (1973) Trans J Br Ceram Soc 72:215
28. Bayer G (1971) J Less-Common Met 24:129
29. Morosin B, Lynch RW (1972) Acta Cryst B28:1040
30. Zhang J, Perez RJ, Lavernia EJ (1993) J Mater Sci 28:2395. doi:10.1007/BF01151671
31. Maekawa Z, Hamada H, Gotoh A, Miyake K (1992) Proceedings of 35th Japan congress on materials research, p 177
32. Daimon K (1990) J Ceram Soc Jpn 98:365
33. Kawaharav K, Yin F (1999) J Vac Soc Japan 42:11